J Arid Land (2025) 17(3): 285–303
doi: 10.1007/s40333-025-0009-7; CSTR: 32276.14.JAL.02500097

Science Press Springer-Verlag

Impact of urban sprawl on land surface temperature in the Mashhad City, Iran: A deep learning and cloud-based remote sensing analysis

Komeh ZINAT[1], Hamzeh SAEID[1], Memarian HADI[2], Attarchi SARA[1], LU Linlin[3,4], Naboureh AMIN[5,6], Alavipanah KAZEM SEYED[1*]

[1] Department of Remote Sensing and GIS (Geographic Information System), University of Tehran, Tehran 14178-53933, Iran;
[2] Department of Watershed Management, University of Birjand, Birjand 97174-34765, Iran;
[3] Key Laboratory of Digital Earth Science, Aerospace Information Research Institute, Chinese Academy of Sciences, Beijing 100094, China;
[4] International Research Center of Big Data for Sustainable Development Goals, Beijing 100094, China;
[5] Research Center for Digital Mountain and Remote Sensing Application, Institute of Mountain Hazards and Environment, Chinese Academy of Sciences, Chengdu 610041, China;
[6] University of Chinese Academy of Sciences, Beijing 100049, China

Abstract: The evolution of land use patterns and the emergence of urban heat islands (UHI) over time are critical issues in city development strategies. This study aims to establish a model that maps the correlation between changes in land use and land surface temperature (LST) in the Mashhad City, northeastern Iran. Employing the Google Earth Engine (GEE) platform, we calculated the LST and extracted land use maps from 1985 to 2020. The convolutional neural network (CNN) approach was utilized to deeply explore the relationship between the LST and land use. The obtained results were compared with the standard machine learning (ML) methods such as support vector machine (SVM), random forest (RF), and linear regression. The results revealed a 1.00°C–2.00°C increase in the LST across various land use categories. This variation in temperature increases across different land use types suggested that, in addition to global warming and climatic changes, temperature rise was strongly influenced by land use changes. The LST surge in built-up lands in the Mashhad City was estimated to be 1.75°C, while forest lands experienced the smallest increase of 1.19°C. The developed CNN demonstrated an overall prediction accuracy of 91.60%, significantly outperforming linear regression and standard ML methods, due to the ability to extract higher level features. Furthermore, the deep neural network (DNN) modeling indicated that the urban lands, comprising 69.57% and 71.34% of the studied area, were projected to experience extreme temperatures above 41.00°C and 42.00°C in the years 2025 and 2030, respectively. In conclusion, the LST predictioin framework, combining the GEE platform and CNN method, provided an effective approach to inform urban planning and to mitigate the impacts of UHI.

Keywords: convolutional neural network; machine learning; Google Earth Engine; land use change; random forest

Citation: Komeh ZINAT, Hamzeh SAEID, Memarian HADI, Attarchi SARA, LU Linlin, Naboureh AMIN, Alavipanah KAZEM SEYED. 2025. Impact of urban sprawl on land surface temperature in the Mashhad City, Iran: A deep learning and cloud-based remote sensing analysis. Journal of Arid Land, 17(3): 285–303. https://doi.org/10.1007/s40333-025-0009-7; https://cstr.cn/32276.14.JAL.02500097

*Corresponding author: Alavipanah KAZEM SEYED (E-mail: salavipa@ut.ac.ir)
Received 2024-09-19; revised 2025-01-14; accepted 2025-01-25

1 Introduction

Land use and land cover (LULC) changes have various consequences on the environment, ecosystem, and human society. These changes play a crucial role in influencing land surface temperature (LST), making it a key element in global warming research and an indicator of climate change acceleration. Anthropogenic activities such as deforestation and urbanization have significantly altered the land surface over the past half century (Jibitha et al., 2024). Rapid transitions in land utilization raise concerns as a significant ecological issue, leading to challenges such as the dwindling of vegetated areas and the emergence of urban heat islands (UHI) effects (Amiri et al., 2009). These changes exert multiple impacts on surface temperatures at both local and global scales (Liu et al., 2022). It is imperative to recognize the upsurge of LST as a critical concern and explore the correlation between land use and LST using a precise approach that considers all relevant factors. This exploration can guide urban planners in developing sustainable urban spaces (Alavipanah et al., 2022).

Comprehensive researches have been directed to recognize the underlying factors affecting the relationship between LULC changes and LST (Nega and Balew, 2022; Khan et al., 2023; Patel et al., 2023; Jibitha et al., 2024). A non-linear correlation between LST and LULC changes has been extensively explored in prior studies, emphasizing the complexity of their interactions (Tran et al., 2017; Wang et al., 2018; Wang et al., 2019b). Tran et al. (2017) highlighted that LST is influenced non-linearly by LULC types. Their methodology, which utilized non-parametric regression and simulated LULC scenarios, demonstrated that UHI patterns are shaped by urban landscape characteristics and development types. However, their approach, although it is effective in forecasting LST patterns, relied heavily on hotspot and regression analyses, which might oversimplify dynamic processes. Similarly, Wang et al. (2018) investigated LULC impacts on LST in Yangon of Myanmar, showing that agricultural practices significantly affect atmospheric and climatic systems. They identified temporal and seasonal variations in LST associated with different land cover types, particularly water bodies and built-up lands, however, their study primarily focused on correlation analysis, leaving room for integrating more advanced methods with non-linear interactions. Wang et al. (2019b) examined spatio-temporal LULC changes in the Pearl River Delta, China using local climate zone (LCZ) classifications. Their findings revealed that urban densification and vertical expansion of low-rise areas contribute significantly to LST increases, but the study relied on LCZ classifications without exploring deeper non-linear relationships. Collectively, these studies underscore the limitation of traditional methods, such as linear regression and correlation analysis, in addressing the intricate and dynamic relationships between LULC changes and LST. This limitation highlights the need for advanced methodologies, like deep learning, to capture complex, non-linear, and spatially heterogeneous interactions, more effectively. Moreover, there are many environmental factors that can affect the relationship between LULC changes and LST. Feng et al. (2019) examined the impacts of three primary factors, i.e. the normalized difference vegetation index (NDVI), the normalized difference built-up index (NDBI), and the normalized difference water index (NDWI), on LST variation. Their findings indicated a significant influence of these indices on LST variation. Similarly, He et al. (2019) utilized Landsat satellite images to explore effect of land characteristics on LST in Chinese mountainous terrains. They found a negative correlation between altitude and LST. They also noted that LST fluctuations were more pronounced in southern exposures, with the vegetation cover being a predominant influencing factor. Patel et al. (2023) analyzed the impact of different land use types on LST using the Landsat image. They found that vegetation indices such as NDVI, along with the indices related to soil moisture and proximity to water bodies, were crucial in regulating LST. The study emphasized that the areas with high vegetation cover exhibited significantly lower LST, while barren lands and urban lands showed elevated LST. Komeh et al. (2023) monitored and compared the spatial autocorrelation of LST with land use in two districts that have dissimilar climate. Results showed that most of the urban lands with temperate climate in coastal areas of the Caspian Sea have high LST, however, the rangelands

have low LST. Zhan et al. (2015) investigated the relationships between LST with land cover ratio and building volume density. Results discovered that there was a strong association between LST and land cover, however, the correlation between LST and building volume density was not significant.

In most studies, classical methods such as linear regression have been used to investigate the relationship between land use change and LST. Nowadays, non-linear procedures and artificial intelligence like deep neural network (DNN) are widely utilized (Ma et al., 2019; Mazzia et al., 2019; Boulze et al., 2020). Recent studies in remote sensing have primarily applied deep learning techniques to generate land use maps. However, these studies often rely on traditional methods, such as linear regression, to analyze the connection between land use changes and LST, rather than using deep learning for this purpose. Therefore, this study applies DNN to capture the complex spatial and non-linear interactions between land use changes and LST. This approach represents a novel application of deep learning in this context, aiming to offer a more precise understanding of these relationships.

DNN types include convolutional neural network (CNN), auto-encoders, recursive neural networks, and recurrent neural networks. Selecting right model and optimizing its parameters is crucial and challenging, significantly impacting the final accuracy. According to the research on remote sensing data analysis, CNNs are highly regarded in image-related applications, with their demonstrated effectiveness in many studies (Zhang et al., 2016; Ma et al., 2019; Li et al., 2024). CNNs have demonstrated strong learning capabilities, particularly when combined with data augmentation techniques like rotation, random noise, and cropping, which prevent overfitting (Gharbia et al., 2020; Naushad et al., 2021). Kussul et al. (2017) applied both one-dimensional (1-D) and two-dimensional (2-D) CNNs to analyze large-scale areas (28×10^3 km^2) using high-resolution free data from Landsat 8 and Sentinel-2 satellites, enabling the discrimination of 11 complex land cover types. The rise of open recognition competitions, such as large-scale visual recognition challenge, has further accelerated the development of CNNs, with the architectures like visual geometry group (VGG), residual neural network (ResNet), and fully convolutional networks (FCN) being adapted for remote sensing applications (Qin et al., 2020; Hao et al., 2023; Li et al., 2024).

This study investigates the patterns of LST in relation to the land use changes in the Mashhad City, Iran from 1985 to 2020. The DNN was developed to model the relationship between LST and land use changes. Using the projections of future land use changes, the CNN model was employed to forecast LST in 2025 and 2030, owing to the capability to solve multifaceted and non-linear problems.

2 Materials and methods

2.1 Study area

The study area is located in the Mashhad City of Khorasan Razavi Province, Iran (36°10′42″–36°24′12″N, 59°26′05″–59°43′36″E; Fig. 1). The city is nestled between the Hezar Masjed and Binaloud mountains. The elevation ranges from 950 to 1150 m a.s.l. The Mashhad City has a cold semi-arid climate with hot, dry summers and cool, somewhat damp winters, receiving around 250 mm of annual precipitation. Temperatures can soar up to 43.00°C in summer, while it can drop to as low as –23.00°C in winter.

2.2 Data source

The Google Earth Engine (GEE) platform was used to process all the steps related to image pre-processing and preparation of the input features. The GEE is a web-based remote sensing platform, which is capable of performing spatial and temporal analyses on multiple satellite image datasets, allowing users to conduct their analysis on geo-big data without requiring a personal processing system (Kumar and Mutanga, 2018; Sidhu et al., 2018). This capability addresses the challenges associated with data loading, storage, and processing encountered in working with big

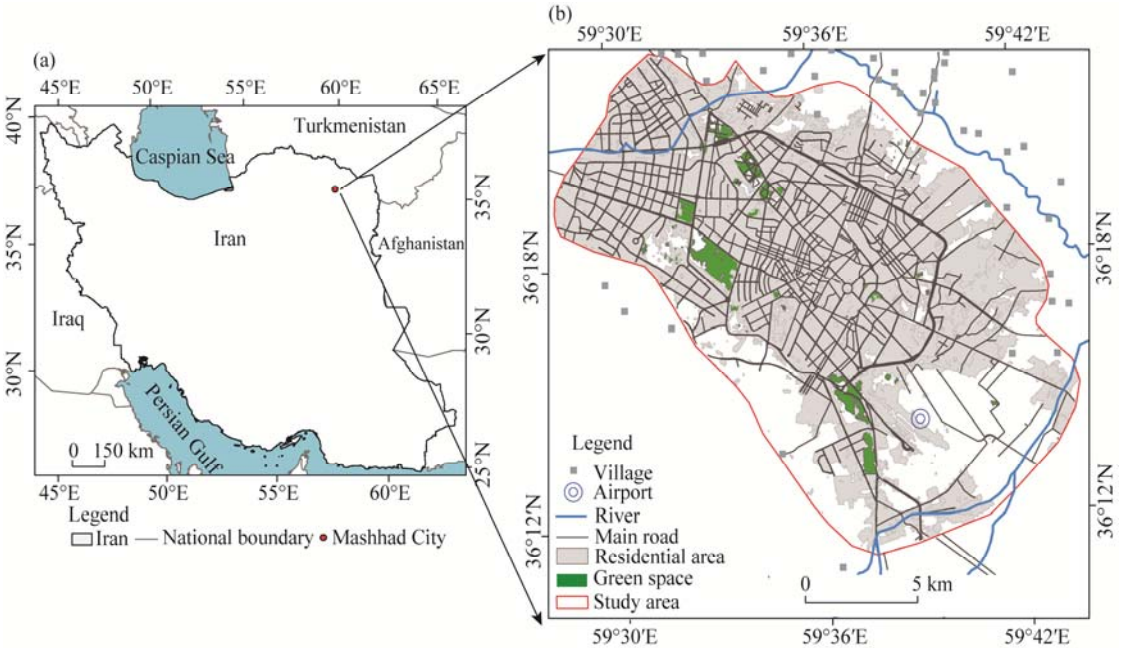

Fig. 1 Geographical location of the Mashhad City (a), Iran and the overview of the city (b)

land surface data (Kumar and Mutanga, 2018; Ravanelli et al., 2018). We made use of a collection of Landsat satellite image chosen for their suitable spectral, spatial, and temporal resolutions, as well as their comprehensive archival record within the period under assessment. In order to avoid the impact of seasonal variations, we utilized images from May, June, and July with the cloud cover under 5.00% to derive land use maps. Consequently, the average summer temperatures for these three months were computed from the images.

2.3 Methods

Figure 2 shows a flowchart of 3 computational steps for data processing and modeling LST. Step 1 involves all the necessary cloud computations in GEE platform; Step 2 implicates the application of the land change modeler (LCM) toolbox for simulating land use maps; and Step 3 comprises the use of deep learning in modeling the relationship between land use and LST.

2.3.1 Land use classification

The land use mapping was facilitated by the object-oriented classification approach, which has been proven to yield significantly a superior precision compared with common pixel-based techniques (Li et al., 2016; Zeraatkar et al., 2021; Wang et al., 2022). Utilizing the support vector machine (SVM) algorithm, we delineated 5 distinct land use types, i.e., built-up lands, forest lands, agricultural lands, barren lands, and rangelands. Typically, this technique involves a two-step process, i.e., segmentation and then classification (Yan, 2003; Memarian et al., 2013). During segmentation, pixels are grouped to separate image objects using spatial and spectral metrics, which are set by the user-defined spectral and geometric properties (Agarwal et al., 2013). Following this, the SVM algorithm is applied for classification purposes. The SVM algorithm is widely recognized for its high classification accuracy and its effectiveness in object-oriented classification, specifically in complex environments (Tzotsos and Argialas, 2008; Puissant et al., 2014).

Object-oriented approach through the SVM algorithm was applied to selected area across 8 temporal intervals. Image classification involved 3 key stages, i.e., initial pre-processing, which encompassed radiometric and atmospheric adjustments as well as contrast enhancement; selection of an appropriate classification technique, determined by a quantitative evaluation of its accuracy; and subsequent post-processing that included the application of majority/minority filters.

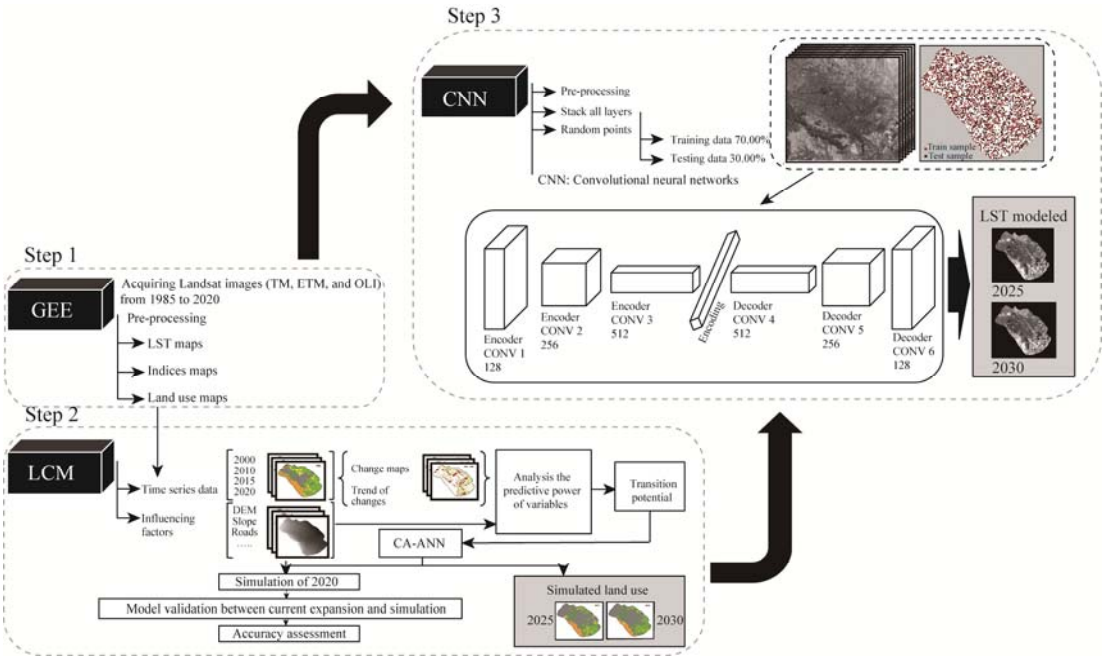

Fig. 2 Data processing framework of the study. GEE, Google Earth Engine; TM, thematic mapper; ETM, enhanced thematic mapper; OLI, operational land imager; LCM, land change modeler; CA-ANN, cellular automata-artificial neural network; CONV, convolutional layer.

2.3.2 LST retrieval

The thermal infrared radiation and physical models have been effectively proven for assessing the temperature over large-scale areas (Wang et al., 2019a). Various techniques have been introduced for analyzing thermal data from different sensors, yet the accuracy of these methods continues to be a subject of ongoing scrutiny. This research utilized the mono-window algorithm to derive and ascertain the LST and to explore its correlation with land use types. The mono-window algorithm necessitates the calculation of average atmospheric temperature, alongside the brightness temperature, emissivity, and Planck's equation, to determine the LST accurately (Rongali et al., 2018). Incorporating the average atmospheric temperature into this formula has been shown to enhance the LST results (Wang et al., 2015; Wang et al., 2019a). The computational steps for extracting the LST are described with details in Komeh et al. (2023).

2.3.3 Land use change simulation

In this study, LCM was used to project land use changes in 2025 and 2030. LCM provides a tool for land cover change assessment and planning. This model proposes a good efficiency in simulating complex land change processes via combining the capabilities of the cellular automata (CA)-Markov chain model with the multi-layer perceptron (MLP) neural network througth error backpropagation training (Eastman, 2009; Tajbakhsh et al., 2018). LCM model is an integrated method that is able to simulate the changes of several land use types simultaneously (Eastman, 2009). In LCM, transition probability matrix and the area of changes are calculated using the Markov chain model. This matrix shows the probability of changing a specific land use to other land use types during the calibration time interval. Based on the major changes that have occurred in the study area, we defined the sub-models of land use transitions. The variables are digital elevation model (DEM), slope, aspect, proximity to residential area, proximity to agricultural land, proximity to forest land, and proximity to road (Christensen and Jokar Arsanjani, 2020), which belongs to static variables. The distances to residential area, road, and agricultural land were considered as dynamic variables and recalculated in several steps.

According to the selected independent variables, we modeled the transition potential of each

land use type through CNN after choosing the sub-models. Because each pixel of the image has the potential to change from one land use type to another, a multi-layer perceptron neural network was used to model the nonlinear relationships between land use change and employed static/dynamic variables. Operationally, the MLP in LCM produces a random sample set of cells that have changed and a set of samples that have remained constant. Based on the utilized spatial variables, the number of neurons in the input layer (n) is equal to the number of variables and the number of neurons in the output layer is equal to the number of changed and consistent land use types. The number of hidden layer neurons is equal to n+1. After obtaining the highest accuracy and the lowest root mean square error (RMSE), and ensuring the grid adjustment, we prepared the transition potential map. Finally, projected land use maps were produced in the years 2025 and 2030.

2.3.4 Land cover indices

There are four main urban elements that can affect the microclimate of a city, i.e., buildings, vegetation, barren land, and water body (Rosenzweig et al., 2008). The intensity of LST is directly related to the degree of urbanization, land use pattern, and the density of buildings (Xiong et al., 2012). Therefore, land cover indicators that are used in many studies to correlate with LST, were employed as auxiliary features in this study (Chen et al., 2006; Liu and Zhang, 2011; Essa et al., 2012; Kafy et al., 2021a). These indices have a linear correlation with LST by a high coefficient of determination (Kafy et al., 2021a). NDVI is a degree of the quantity of vegetation on the land surface, which is connected with the vigor of vegetation, due to more energy reflectance of the healthy vegetation than unhealthy and sparse vegetation. NDVI values differ between 1 and –1. Higher NDVI values specify dense and improved vegetation, while lower values designate poorer vegetation (Taloor et al., 2021). The spaces with water bodies and rivers show higher values of NDWI compared with the areas without water bodies/rivers. NDBI is a spectral metric to obtain a trustworthy and valid relationship between LST and built-up lands in a city (Guha et al., 2020). The application of these indices has been proven in many studies to investigate LST effectively (Malik et al., 2019; Shahfahad Kumari et al., 2020; Taloor et al., 2021; Alademomi et al., 2022; Alavipanah et al., 2022). LULC indicators including NDVI, NDBI, and NDWI were calculated using the red spectral bands, shortwave infrared, and near-infrared spectral bands (Abutaleb et al., 2015; Yengoh et al., 2015; Gascon et al., 2016; Arekhi et al., 2019).

In this work, three widely recognized land use indices including NDVI, NDBI and NDWI were utilized. These indices were selected as they effectively represent vegetation cover, urban development, and water bodies, which are critical components influencing LST variations. This approach certified a more detailed and robust investigation of the relationship between land use changes and LST, offering insights that traditional methods might not capture. All these indicators for the studied intervals were extracted through the GEE platform and used as supporting features in the CNN.

2.3.5 Modeling relationship between land use and LST

In this study, we utilized ML algorithms to analyze data, learn, and make informed decisions based on what they have learned. The deep learning procedures were used to extract features from the input data and to add supplementary information from the investigated variables to achieve a higher accuracy in results. The deep learning as one of the subsets of artificial intelligence, is a construction of ML algorithms, which is engaged for the hierarchical representational learning of data. The concept of deep learning originates from CNN, which is multi-layered structures of perceptrons with several hidden layers (Hinton and Salakhutdinov, 2006; Günen, 2022). In DNN, it is possible to enter more complex relationships to achieve improved results.

Based on the studies conducted for remote sensing data analysis, among different architectures, CNN is one of the most famous neural networks in image-related application, whose performance has been proven in various researches (Adam et al., 2014; Maxwell et al., 2018; Wang et al., 2022). Typically, a CNN is structured into three primary layers, i.e., convolution layer, pooling

layer, and fully connected layer, with distinct function for each layer (Shin et al., 2016). The training process of a CNN involves two main phases, i.e. the feed-forward phase and the back-propagation phase. During the feed-forward phase, the input image undergoes a series of point multiplications with neuron parameters, followed by convolution operations across each layer, culminating in the computation of the network's output. Subsequently, the network's parameters are fine-tuned, or trained, by utilizing the output values to determine the network's error margin. This process is achieved by comparing the network's output to the correct answer through an error function. Following the computation of the error, the subsequent phase is the back-propagation process. During this phase, the gradient for each parameter is determined using the chain rule. Then we made adjustments to all parameters based on their contribution to the network's error. Once the parameters are adjusted, the feed-forward process is initiated again. This cycle of steps is repeated until the network achieves the required level of precision, in which the training is considered complete. Essentially, a CNN is a layered neural network, where convolutional layers alternate with pooling layers, leading up to several fully connected layers. Within the convolutional layer, the CNN employs a variety of kernels to process the input image and map out intermediate features, creating a range of feature maps. Typically, a pooling layer follows a convolutional layer to diminish the dimensions of the feature maps and the number of network parameters. Pooling layers maintain stability in the face of positional changes, due to their processing of adjacent pixel values. The most prevalent forms of pooling are max pooling and average pooling. Subsequently, fully connected layers convert the two-dimensional feature map into a one-dimensional feature vector, facilitating the continuation of the feature representation process (Wang et al., 2019c; Fang et al., 2020). The theoretical underpinnings and formulas of deep convolutional neural networks are extensively documented in several researches (Rezaee et al., 2018; Mazzia et al., 2019; Boulze et al., 2020).

The overall structure and architecture of the designed network is shown in Step 3 (Fig. 2). The designed network was comprised of two general parts. In the first part, a total of 3 layers were used. The initial layer was responsible for mining low-level features and the final layer was in charge to extract higher-level features. All 3 layers were composed of convolution layer, batch normalization layer, and activation function, respectively. Convolutional layers employed three dimensions (3D) kernels for feature extraction. Therefore, the network was able to simultaneously present the spatial and temporal characteristics of each image pixel and utilized them in the final decision (Li et al., 2017). It should be noted that in order to deepen the network learning by increasing the number of convolutional layers, the output dimensions of each convolution layer were considered similar to its input dimensions, by means of the layering technique. The number of filters employed in 3 layers was respectively obtained to be 128, 256, and 512 using the trial-and-error approach to find the highest accuracy. The output of the convolutional layer was normalized by the batch normalization layer, with the aim of facilitating training, preventing overfitting, and generalizing the network as much as possible (Ioffe and Szegedy, 2015; Zhao et al., 2019). The output of the batch normalization layer was prepared to enter the next layer by the rectified linear unit (ReLu) nonlinear function with the purpose of empowering the network in modeling nonlinear relationships. In addition to the high speed in the error back-propagation process, the ReLu function is known as the most common activation function used in convolutional networks.

In addition to the above layers, a 2×2×2 max pooling layer was used, whose input is the output of the ReLu activation function. These dimensions were chosen as the most widely used ones of the max pooling layer in various researches (Krizhevsky et al., 2012; Zhao et al., 2019). Besides reducing the volume of calculations and maintaining the extracted main features, max pooling layer facilitates network training by decreasing the number of network connections and reducing the number of parameters that can be trained in the network (Guidici and Clark, 2017).

All stages of designing, implementing, training and evaluating the accuracy of the desired network was done within the Keras deep learing library in Python. To train the network, we used the cost function of cross-entropy as the chief cost function in classification applications (Mazzia

et al., 2019; Boulze et al., 2020). The network was trained in 1000 iterations to find the minimum value of the cost function via the gradient descent optimization algorithm. The optimal learning rate was also chosen among the values of 0.10000, 0.0100, 0.0010, and 0.0001 through the network search method to obtain the highest final accuracy on the validation data set (Carranza-García et al., 2019).

2.4 Accuracy assessment

The accuracy evaluation of the proposed method and comparison of its performance with other procedures was performed by using the confusion matrix and overall accuracy measure. The performance evaluation was accomplished in two stages. In the first stage, the classification accuracy of the predicted maps was evaluated. In the second stage, the proposed method was compared with the other two standard approaches of machine learning, i.e., random forest (RF) and support vector machine (SVM).

2.4.1 RF

The RF consists of multiple decision trees to achieve a goal, and is used for classification and regression prediction (Breiman, 2001; Lausch et al., 2017). The bootstrap sampling method was applied in this work to conduct random sampling with replacement of the samples. Each sampling result was used to construct a regression tree, and multiple decision trees were combined to form the RF model. The variables were screened and classified utilizing the model to predict the unknown parameters. The RF model does not require the assumption of a prior probability distribution. Therefore, it has good flexibility and stability, as well as high computation speed and accuracy (Naidoo et al., 2019).

2.4.2 SVM

No assumption is required in the SVM model for the underlying data distribution and dimensions of the input space. The SVM provides a group of classified data samples (Vaglio Laurin et al., 2016). In addition, the SVM is applied to regression, which is known as support-vector regression (SVR). Numerous existing studies have applied SVR to remote-sensing quantitative estimations (Camps-Valls et al., 2006; Du et al., 2018).

The RF and SVM methods have their own input parameters. Network search technique was employed to search among the parameters number of trees with the values of 100, 200, 300, and 400, the depth with the values of 4, 6, 8, 10, and 12, the kernel type (radial or linear) and also the cost (C) coefficient with the values of 0.1, 1.0, 10.0, and 100.0 to find the optimum values for each. It should be noted that both the RF and SVM methods have other input parameters. According to the investigations, the impact of changing these parameters on the final result is very minor. Therefore, the study was only carried out for the parameters that had a significant impact on the final result (Axelsson et al., 2013).

The employed methods were evaluated each time with 1000 repetitions, due to the usage of training data and various evaluations in each implementation. The training and validation analysis of the employed methods with different datasets in each execution causes a fairer assessment of the presented model and provides a more accurate comparison of its performance with other models. It should be noted that the ground data (collected based on field survey) is randomly divided into two groups of validation and training data at the percentages of 30.00% and 70.00%, respectively, in each implementation. This work prevents the possible overfitting of the designed network.

3 Results

3.1 LULC changes

Land use patterns in the Mashhad City are depicted in Figure 3. Accuracy assessment of the classified land use maps with 300 ground points was completed using the global positioning system (GPS) and GEE platform. The results of validation analysis of the land use maps are given

in Table 1 and the diagrams are shown in Figure 4. The producer accuracy and user accuracy are displayed for each class, providing a clear comparison between the model's ability to classify samples correctly and the reliability of those classifications. The results from Table 1 and Figure 4 collectively demonstrate the strong performance of the classification methodology across all studied time periods. While there are minor fluctuations in certain land use types, the overall accuracy metrics and class-wise trends indicate that the generated land use maps were reliable and suitable for further analysis. These results confirmed the effectiveness of the approach in capturing the dynamics of land use changes over time. Figure 5 shows the area change of each land use in different years. In 1985, the largest area of land use belongs to agricultural land, while, in 2020, built-up land covers the largest area. In other words, the areas of rangeland, agricultural land, and barren land were reduced by 14.50%, 13.00% and 10.00%, respectively.

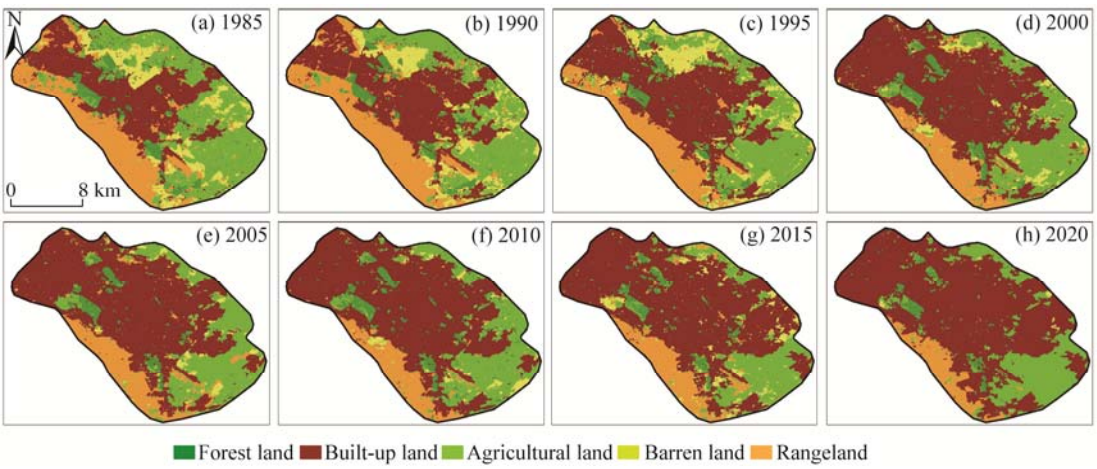

Fig. 3 Changes of different land use types of the Mashhad City from 1985 to 2020. (a), 1985; (b), 1990; (c), 1995; (d), 2000; (e), 2005; (f), 2010; (g), 2015; (h), 2020.

Table 1 Accuracy measurement for the generated land use dataset

Accuracy	1985	1990	1995	2000	2005	2010	2015	2020
Overall accuracy (%)	92.70	89.40	91.00	91.20	91.90	91.00	96.90	94.00
PA (%)	90.00	87.60	91.40	86.80	92.60	92.40	96.60	93.60
UA (%)	88.60	90.00	91.00	89.60	92.60	91.00	96.60	94.20

Note: PA, producer accuracy; UA, user accuracy.

3.2 Land use change simulation

The extent of changes for each land use was extracted using the proposed Markovian model and the LCM toolbox within the TerrSet software. Finally, the projected land use maps in the years 2025 and 2030 were acquired (Fig. 6). For this purpose, the ANN-based CA-Markov model was firstly used to simulate the land use in 2020, then the results were validated via comparing the observed and predicted maps. The simulated results indicated that if the current growth of built-up lands persists without any rational planning, these areas will expand further in the years 2025 and 2030, which account for 69.57% and 71.34% of the total area, respectively. This trend will result in the reduction of agricultural land and rangeland with urban expansion.

3.3 LST changes

The process of identifying the changes in various land use types and subsequently calculating LST for a specific time was performed within GEE platform. LST results are depicted in Figure 7. In 1985, the highest recorded temperature was 43.21°C, which increased up to 44.73°C in 2020.

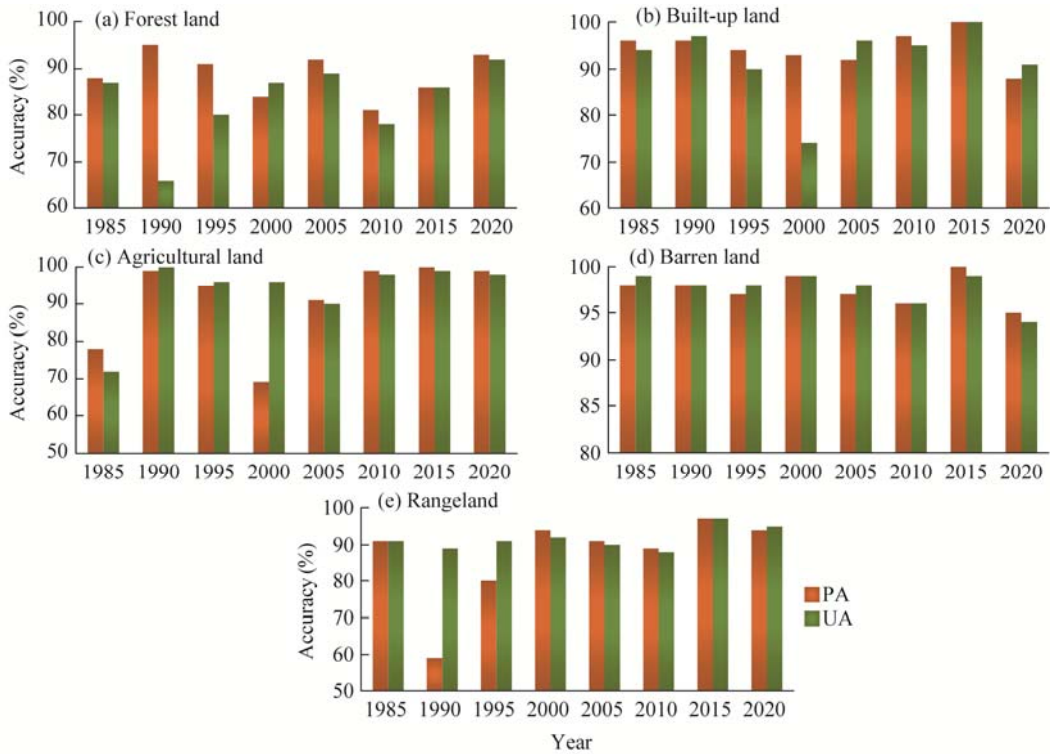

Fig. 4 Producer accuracy (PA) and user accuracy (UA) metrics for different land use types from 1985 to 2020. (a), forest land, (b), built-up land; (c), agricultural land; (d), barren land; (e), rangeland.

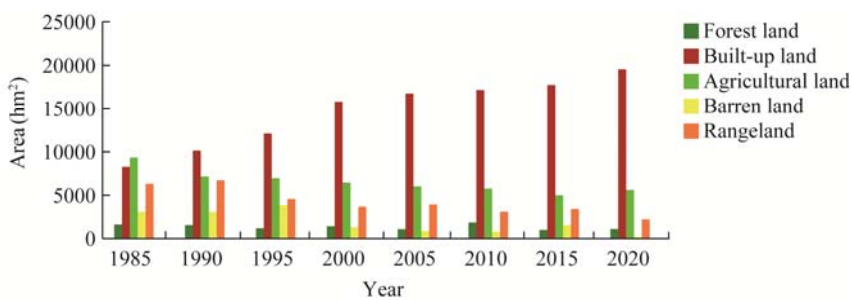

Fig. 5 Area changes of different land use types of the Mashhad City from 1985 to 2020

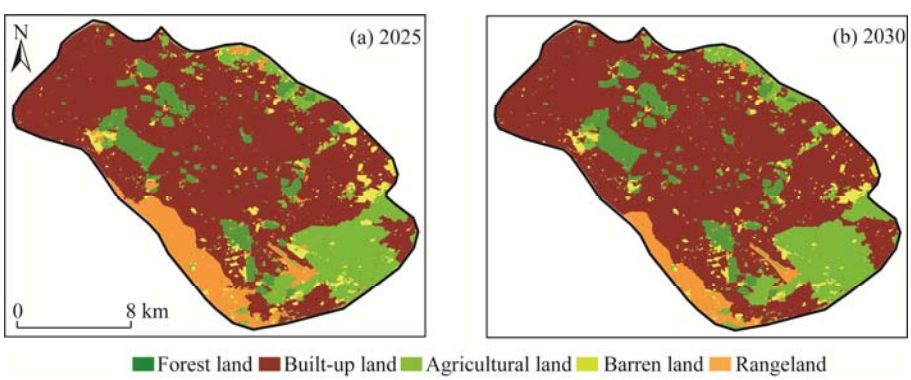

Fig. 6 Projected map of different land use types in the years 2025 (a) and 2030 (b)

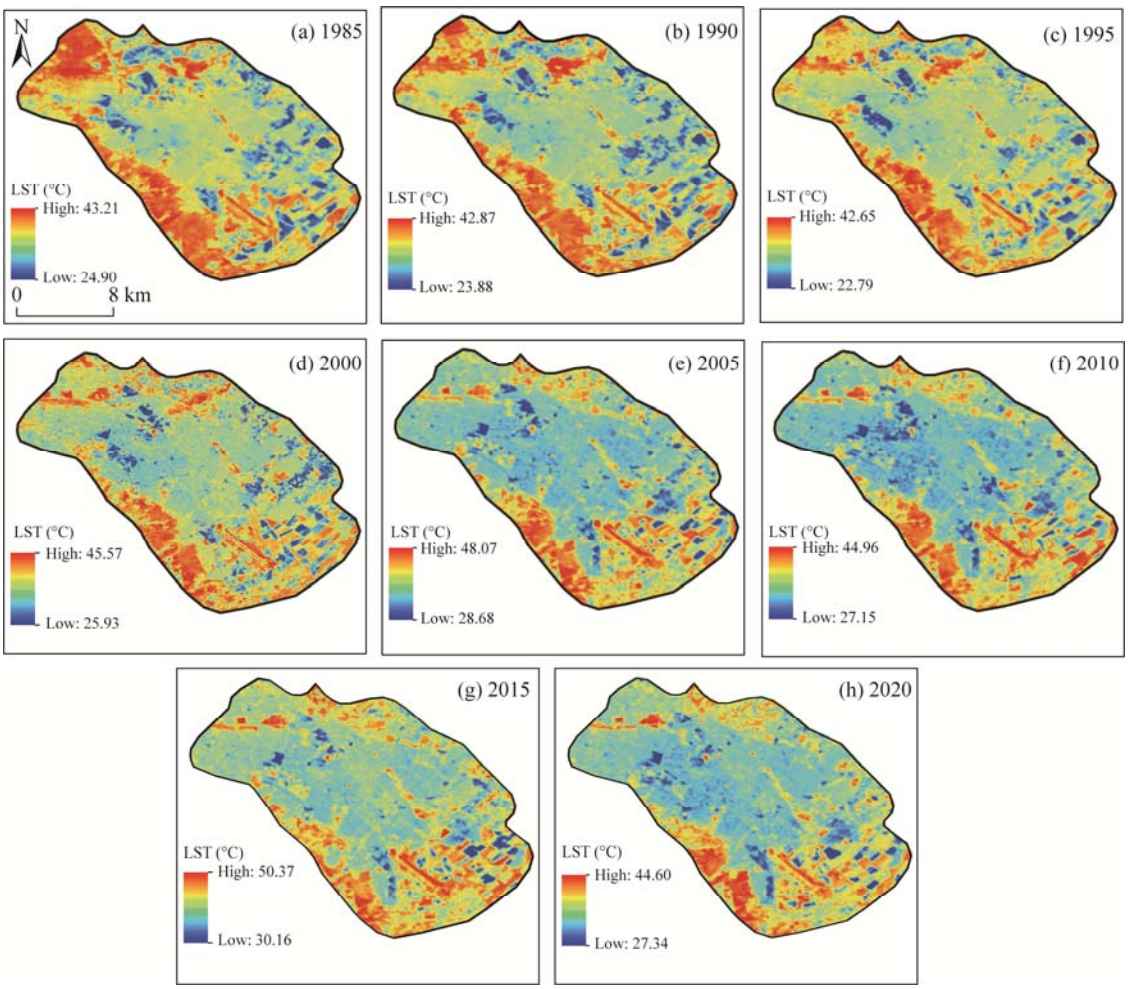

Fig. 7 Land surface temperature (LST) maps of the Mashhad City from 1985 to 2020. (a), 1985; (b), 1990; (c), 1995; (d), 2000; (e), 2005; (f), 2010; (g), 2015; (h), 2020.

Similarly, the lowest temperature of 24.90°C was recorded in 1985, which increased significantly up to 27.34°C in 2020. According to the results, the Mashhad City experienced an average temperature increase of 1.75°C (Fig. 8). Additionally, by means of correlating the average LST with the dynamics of land use throughout the study period, it was indicated that the temperature rise varied among different land use types. In urbanized districts, the temperature increase was calculated to be around 1.75°C. Consequently, the mean summer temperature in the urbanized areas of the Mashhad City escalated from 34.50°C in 1985 to 36.25°C in 2020. In contrast, rangeland also experienced a temperature rise of 1.75°C, while the smallest increment was observed in forest land, registering a rise of 1.19°C (Fig. 8).

3.4 Modelling process of temperature

After modeling the relationship between LULC and LST using the CNN, the predicted LULC maps in the years 2025 and 2030 were utilized to generate their corresponding LST maps. Figure 9 shows the predicted LST maps of 2025 and 2030. Based on the obtained results, the majority of the studied area will have temperatures above 41.00°C and 42.00°C for the years 2025 and 2030, respectively. Moreover, the simulated average LST for residential areas will be 40.00°C and 43.00°C, respectively.

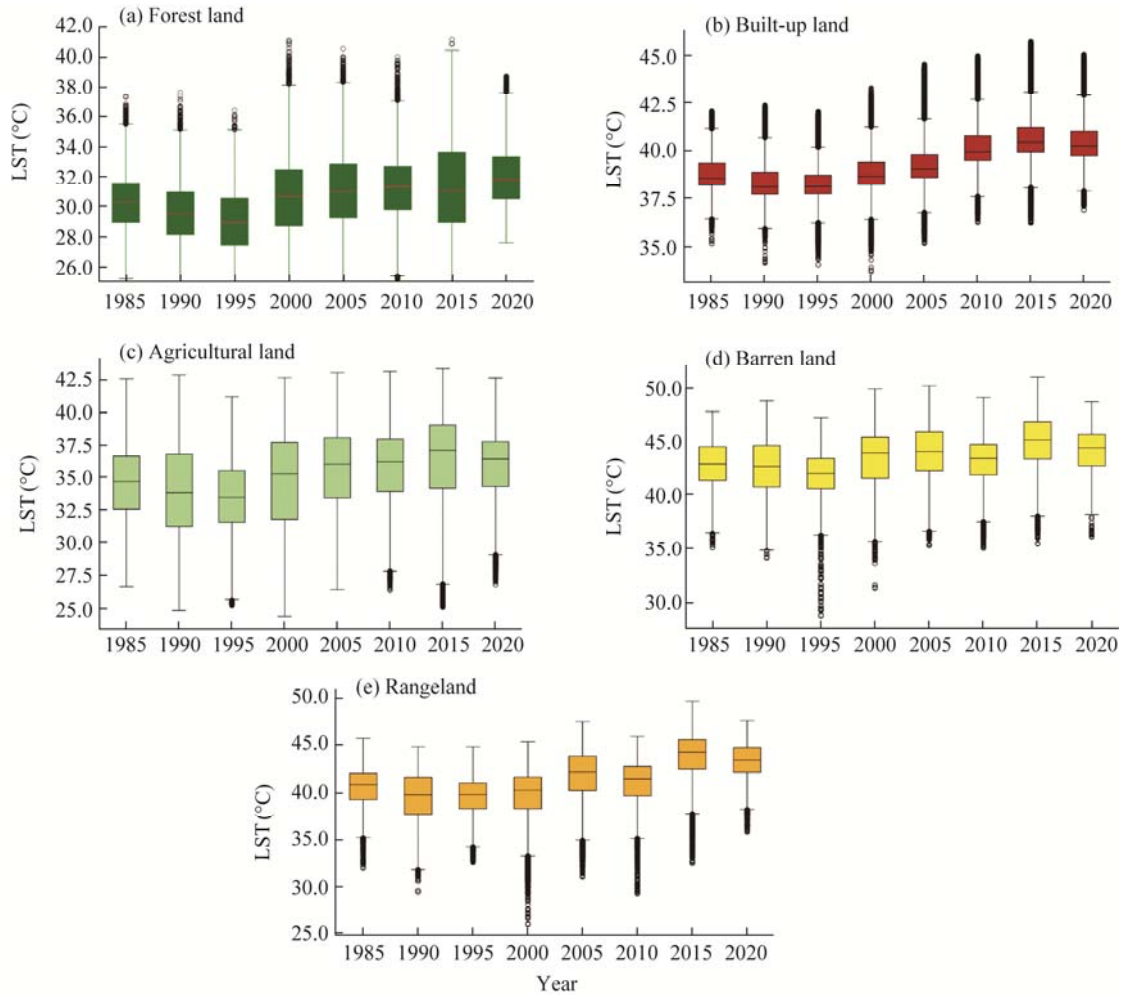

Fig. 8 Box plots of LST for different land use types from 1985 to 2020. (a), forest land; (b), built-up land; (c), agricultural land; (d), barren land; (e), rangeland. Boxes indicate the IQR (interquartile range, 75th to 25th of the data). The median value is shown as a line within the box. Outlier is shown as black circle. Bars extend to the most extreme value within 1.5×IQR.

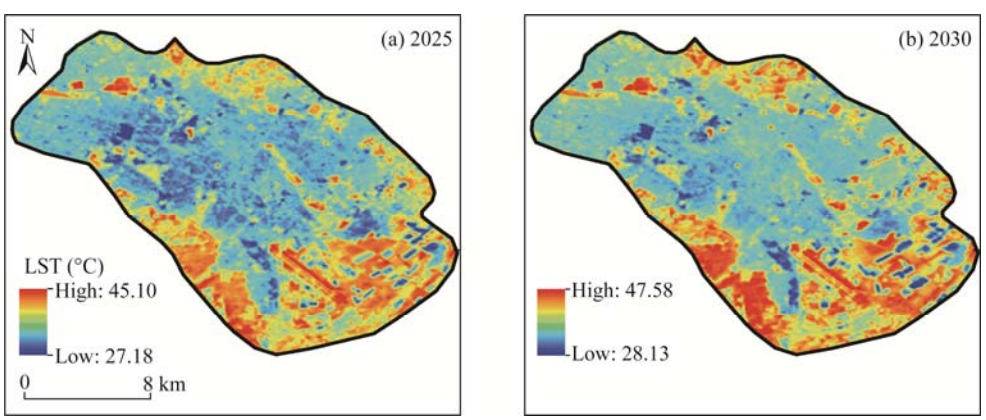

Fig. 9 LST maps simulated using the convolutional neural network (CNN) in the years 2025 (a) and 2030 (b)

3.5 Accuracy of simulated LST map

The validity of LST simulated maps was analyzed using the determination of coefficient (R^2) and

mean squared error (MSE) via a comparison between the predicted and observed LST for the year 2020. The DL method established a good fit according to the R^2 and MSE of 0.914 and 0.31°C, respectively (Fig. 10).

Additionally, to compare the proposed method, these parameters were also calculated for the RF and SVM methods. It is worth noting that these two methods have their own specific parameters, which were optimized during the analysis. The optimal performance of the RF method was acquired by 300 trees and the maximum depth of 10. Furthermore, the optimum performance for the SVM was obtained through a radial kernel with a coefficient of cost equal to 10.

The CNN method with an average accuracy of 91.60%, has performed better than other methods. In Figure 10, the CNN method showed the closest alignment, with the most points clustered near the trend line, particularly in the 32.00°C–40.00°C range, suggesting the highest accuracy. Among the investigated methods, the linear regression was ranked the lowest average accuracy (73.73%) and the greatest scattering, indicating a weaker correlation. The designed DNN method resulted in a better accuracy than the two known ML methods, i.e., RF and SVM, due to the ability of extracting higher level features. The methods of RF and SVM were ranked the second and third respectively with the average accuracies of 86.23% and 85.80% (Fig. 10). These results highlight a significant variability in the predictive power of the employed methods.

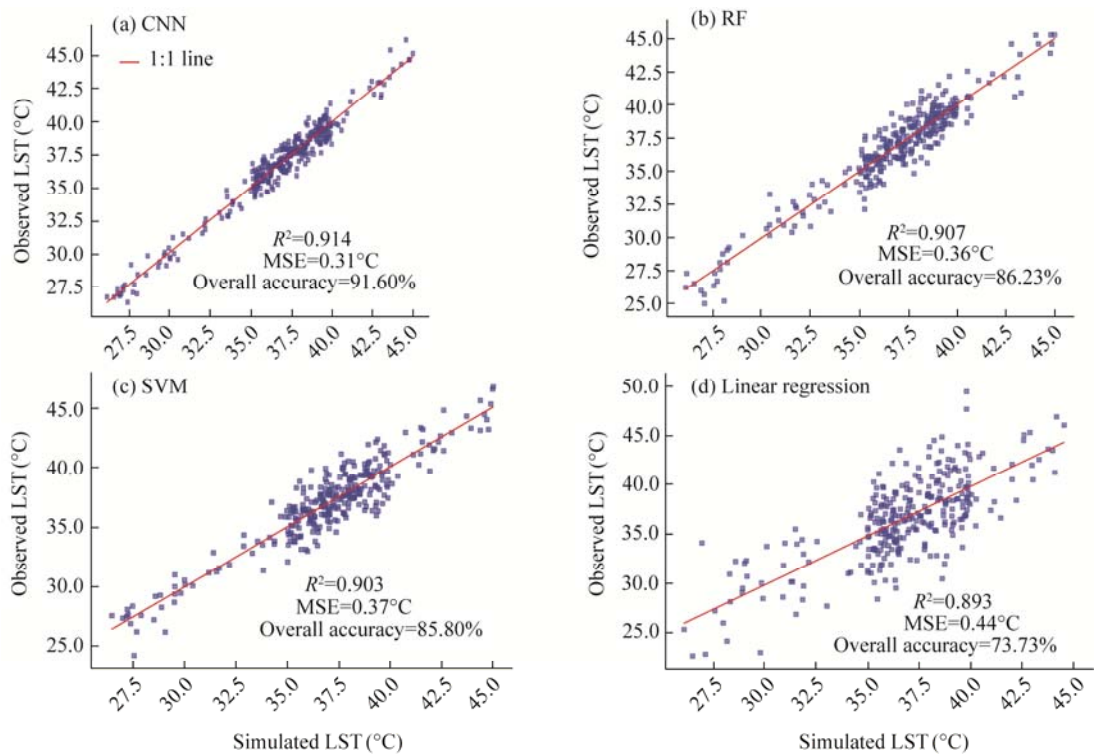

Fig. 10 Correlation between simulated and observed LST for the year 2020 using four different methods. (a), CNN; (b), random forest (RF); (c), support vector machine (SVM); (d), linear regression. R^2, determination of coefficient; MSE, mean squared error.

4 Discussion

Based on the results obtained from the analysis of land use change detection in the Mashhad City, the reduction in agricultural land area and the increase in built-up land area clearly indicated the city's sprawl and its conversion into other land uses (Tajbakhsh et al., 2016; Komeh et al., 2023). Furthermore, several factors, including uncontrolled migration, unplanned expansion to deal with

the increase in urban population, and indiscriminate development of infrastructure, may all play a significant role in these urban sprawls. The underlying hypothesis suggests that this substantial urban growth is driven by strategic and economic factors that lead to a lack of increasing land cover such as green spaces and water bodies (Fu and Weng, 2018; Kafy et al., 2021a).

Decreased vegetation cover and intensified urbanization may affect the city's ecosystem services, urban health, and thermal properties. If the unplanned urban growth continues, the UHI effects will likely intensify and result in economical, environmental, and health problems (Kafy et al., 2021b). Appropriate planning of land use, protection of water bodies, afforestation, and growth of urban green spaces assists to make the city of Mashhad more sustainable by reducing the impacts of UHI. The results also confirmed that the increasing trend of LST in recent years (1985–2020) was consistent with the increase of constructions. Furthermore, this trend of expanding urban areas and reduction of vegetation cover in the Mashhad City intensified the UHI impacts. The temperature increases were most pronounced in the areas where vegetation was diminished or eradicated, specifically in the land use transitions of forest lands and agricultural lands to urban and barren lands. On the other hand, in the areas where forest lands and agricultural lands were expanded, the rise in temperature was mitigated to the lowest levels, as illustrated in Figure 8. The higher LST occurred in the rangelands surrounding the city, compared with the urban lands. The reason is that the presence of barren lands in the area with a hot and dry climate, which heats up quickly during the day, resulting in the higher temperature (Lazzarini et al., 2013; Rasul et al., 2015). The research by Alavipanah et al. (2014) also found that the most important factor in the expansion of heat islands in the Mashhad City was the reduction of vegetation cover. Despite of the issue of urbanization, other possible causes, e.g., the increase in greenhouse gas emissions and the warming of the surface Earth, can also result in temperature increase (Alavipanah et al., 2022). The result was also consistent with other associated remote sensing studies, which deep learning was a powerful modeling technique for nonlinear and complex datasets (Schmidhuber, 2015). The projected LST showed the consequence of temperature increase at the current trend, including the effects of a higher expension of UHI. The further increase in the greenhouse gas emissions harms human well-being, degrades the quality of urban health, and consequently reduces the environmental sustainability of the city (Kafy et al., 2021b). Moreover, increasing the temperature and especially increasing the minimum temperature can affect the amount of evapotranspiration and future snowfall in the area. Certainly these hydro-climatic changes will affect the biodiversity of the watershed (Rahimpour et al., 2021).

The use of NDVI, NDBI, and NDWI as auxiliary variables in the CNN model played a significant role in capturing the spatial heterogeneity of land use patterns and also their impacts on LST variations. Through comparing the CNN method with other machine learning approaches, we foung that the CNN model had superior accuracy in exploring the intricate spatial patterns and establishing the relationships between LST and LULC. This improvement is attributed to the CNN's layered architecture, which allows for an automatic learning of spatial features, making it more capable of handling spatial dependencies and variations (Feng et al., 2019).

It is necessary to mention that the greenhouse impacts and global warming in surface features are also the main reasons that affect the increase in LST even in the areas without significant urbanization (Aslan and Koc-San, 2023; Munawar et al., 2023). As confirmed in the IPCC (Intergovernmental Panel on Climate Change, 2014), the Asian area is facing a temperature rise that is higher than the global average. The heat capacity of LULC is affected by the increase in LST, which leads to the formation of UHIs. The UHI phenomenon poses significant environmental challenges, which negatively affect human health and biodiversity on the broader ecosystem, as highlighted by Grimmond (2007). The impact of UHI and global warming can be significantly reduced by planting urban vegetation around building blocks and forming green rooftops (Pérez et al., 2017).

While this study primarily focused on NDVI, NDBI, and NDWI as the key environmental factors on LST modeling, the findings demonstrate the feasibility of extending this framework to include additional climatic and environmental variables, such as humidity, precipitation, and soil

moisture in the future research. By incorporating these variables, future studies can provide a more comprehensive understanding of the multifaceted interactions influencing LST. This approach not only validates the application of CNNs in modeling complex relationships but also highlights their potential for addressing diverse environmental challenges through improved spatial analysis and predictive capabilities.

Despite the promising findings, this study has some limitations. First, although the analysis primarily focused on NDVI, NDBI, and NDWI as auxiliary variables, incorporating additional factors such as latitude and climatic and environmental variables could potentially yield even more accurate and comprehensive results. Second, the CNN model demonstrated superior performance, however, its computational intensity and longer processing time remain challenges for applying this framework to larger areas or datasets with higher temporal resolution. Future research should address these aspects to enhance the robustness and scalability of the methodology.

5 Conclusions

The study examined the variations in LST and its association with the conversion in land use types in the Mashhad City, Iran from 1985 to 2020. In the last 35 a, Mashhad City has experienced significant urban growth, leading to substantial changes in the land use types. It was observed that the rise in temperature, which ranged from 1.00°C to 2.00°C, corresponded with the land use alterations. Moreover, the expansion of bulid-up lands was still continued. The expansion of built-up lands was mainly associated with the decreases of rangelands, agricultural lands, and barren lands, and the LST in built-up lands was observed to be at its highest level. According to the simulation results, we found that the built-up lands will expand further in 2025 and 2030.

To model the relationship between land use and LST, we found that the application of CNN had a higher accuracy compared with the other methods. The urban land areas will have temperatures above 41.00°C and 42.00°C for the years 2025 and 2030, respectively, throught the simulation result of CNN. It is suggested that future researches investigate the application of proposed method in diverse climatic areas, incorporating a wider range of environmental factors to enhance its validation and adaptability. Moreover, the development of new architectures based on alternative neural networks, such as recurrent neural networks, could provide valuable insights and further improvements for future studies.

Conflict of interest

The authors declare that they have no known competing financial interests or personal relationships that could have appeared to influence the work reported in this paper.

Author contributions

Writing - original draft preparation: Komeh ZINAT; Methodology: Hamzeh SAEID; Writing - review and editing: Memarian HADI, Attarchi SARA, LU Linlin, Naboureh AMIN; Superversion: Memarian HADI, Attarchi SARA, Alavipanah KAZEM SEYED; Formal analysis and investigation: Alavipanah KAZEM SEYED. All authors approved the manuscript.

References

Abutaleb K, Ngie A, Darwish A, et al. 2015. Assessment of urban heat island using remotely sensed imagery over Greater Cairo, Egypt. Advances in Remote Sensing, 4(1): 35–47.

Adam E, Mutanga O, Odindi J, et al. 2014. Land-use/cover classification in a heterogeneous coastal landscape using RapidEye imagery: Evaluating the performance of random forest and support vector machines classifiers. International Journal of Remote Sensing, 35(10): 3440–3458.

Agarwal S, Vailshery L S, Jaganmohan M, et al. 2013. Mapping urban tree species using very high resolution satellite imagery: Comparing pixel-based and object-based approaches. ISPRS International Journal of Geo-Information, 2(1): 220–236.

Alademomi A S, Okolie C J, Daramola O E, et al. 2022. The interrelationship between LST, NDVI, NDBI, and land cover change in a section of Lagos metropolis, Nigeria. Applied Geomatics, 14(2): 299–314.

Alavipanah S K, Darrehbadami S H, Kazemzadeh A. 2014. Spatial-temporal analysis of urban heat-island of Mashhad City due to land use/cover changes and expansion. Geographical Urban Planning Research, 3(1): 1–17. (in Persian)

Alavipanah S K, Mansourmoghaddam M, Gomeh Z, et al. 2022. The reciprocal effect of global warming and climatic change (new perspective): A review. Desert, 27(2): 291–305.

Amiri R, Weng Q H, Alimohammadi A, et al. 2009. Spatial–temporal dynamics of land surface temperature in relation to fractional vegetation cover and land use/cover in the Tabriz urban area, Iran. Remote Sensing of Environment, 113(12): 2606–2617.

Arekhi M, Goksel C, Balik Sanli F, et al. 2019. Comparative evaluation of the spectral and spatial consistency of Sentinel-2 and Landsat-8 OLI data for Igneada longos forest. ISPRS International Journal of Geo-Information, 8(2): 56, doi: 10.3390/ijgi8020056.

Aslan N, Koc-San D. 2023. The effects of land cover changes on land surface temperatures. The International Archives of the Photogrammetry, Remote Sensing and Spatial Information Sciences, 48: 1311–1318.

Axelsson C, Skidmore A K, Schlerf M, et al. 2013. Hyperspectral analysis of mangrove foliar chemistry using PLSR and support vector regression. International Journal of Remote Sensing, 34(5): 1724–1743.

Boulze H, Korosov A, Brajard J. 2020. Classification of sea ice types in Sentinel-1 SAR data using convolutional neural networks. Remote Sensing, 12(13): 2165, doi: 10.3390/rs12132165.

Breiman L. 2001. Random forests. Machine Learning, 45: 5–32.

Camps-Valls G, Gómez-Chova L, Muñoz-Marí J, et al. 2006. Retrieval of oceanic chlorophyll concentration with relevance vector machines. Remote Sensing of Environment, 105(1): 23–33.

Carranza-García M, García-Gutiérrez J, Riquelme J C. 2019. A framework for evaluating land use and land cover classification using convolutional neural networks. Remote Sensing, 11(3): 274, doi: 10.3390/rs11030274.

Chen X L, Zhao H M, Li P X, et al. 2006. Remote sensing image-based analysis of the relationship between urban heat island and land use/cover changes. Remote Sensing of Environment, 104(2): 133–146.

Christensen M, Jokar Arsanjani J. 2020. Stimulating implementation of sustainable development goals and conservation action: Predicting future land use/cover change in Virunga National Park, Congo. Sustainability, 12(4): 1570, doi: 10.3390/su12041570.

Du H Q, Mao F J, Zhou G M, et al. 2018. Estimating and analyzing the spatiotemporal pattern of aboveground carbon in bamboo forest by combining remote sensing data and improved biome-bgc model. IEEE Journal of Selected Topics in Applied Earth Observations and Remote Sensing, 11(7): 2282–2295.

Eastman J R. 2009. IDRISI Taiga Guide to GIS and Image Processing. Worcester: Clark University.

Essa W, Verbeiren B, van der Kwast J, et al. 2012. Evaluation of the DisTrad thermal sharpening methodology for urban areas. International Journal of Applied Earth Observation and Geoinformation, 19: 163–172.

Fang Z C, Wang Y, Peng L, et al. 2020. Integration of convolutional neural network and conventional machine learning classifiers for landslide susceptibility mapping. Computers & Geosciences, 139: 104470, doi: 10.1016/j.cageo.2020.104470.

Feng Y J, Gao C, Tong X H, et al. 2019. Spatial patterns of land surface temperature and their influencing factors: A case study in Suzhou, China. Remote Sensing, 11(2): 182, doi: 10.3390/rs11020182.

Fu P, Weng Q H. 2018. Responses of urban heat island in Atlanta to different land-use scenarios. Theoretical and Applied Climatology, 133: 123–135.

Gascon M, Cirach M, Martínez D, et al. 2016. Normalized difference vegetation index (NDVI) as a marker of surrounding greenness in epidemiological studies: The case of Barcelona city. Urban Forestry & Urban Greening, 19: 88–94.

Gharbia R, Khalifa N E M, Hassanien A E. 2020. Land cover classification using deep convolutional neural networks. In: Abraham A, Piuri V, Gandhi N, et al. Advances in Intelligent Systems and Computing. Switzerland: Springer, 911–920.

Grimmond S. 2007. Urbanization and global environmental change: local effects of urban warming. The Geographical Journal, 173(1): 83–88.

Guha S, Govil H, Gill N, et al. 2020. Analytical study on the relationship between land surface temperature and land use/land cover indices. Annals of GIS, 26(2): 201–216.

Guidici D, Clark M L. 2017. One-dimensional convolutional neural network land-cover classification of multi-seasonal hyperspectral imagery in the San Francisco Bay Area, California. Remote Sensing, 9(6): 629, doi: 10.3390/rs9060629.

Günen M A. 2022. Performance comparison of deep learning and machine learning methods in determining wetland water areas using EuroSAT dataset. Environmental Science and Pollution Research, 29(14): 21092–21106.

Hao X J, Liu L, Yang R J, et al. 2023. A review of data augmentation methods of remote sensing image target recognition.

Remote Sensing, 15(3): 827, doi: 10.3390/rs15030827.

He J L, Zhao W, Li A N, et al. 2019. The impact of the terrain effect on land surface temperature variation based on Landsat-8 observations in mountainous areas. International Journal of Remote Sensing, 40(5–6): 1808–1827.

Hinton G E, Salakhutdinov R R. 2006. Reducing the dimensionality of data with neural networks. Science, 313(5786): 504–507.

Ioffe S, Szegedy C. 2015. Batch normalization: Accelerating deep network training by reducing internal covariate shift. In: Bach F, Blei D. Proceedings of the 32nd International Conference on International Conference on Machine Learning. France: PMLR, 448–456.

IPCC (Intergovernmental Panel on Climate Change). 2014. Mitigation of climate change. Contribution of working group III to the fifth assessment report of the intergovernmental panel on climate change, 1454: 147, doi: 10.1017/CBO9781107415416.

Jibitha J B, Achu A L, Joseph S, et al. 2024. Assessment of changes in land use/land cover and land surface temperature in a fast-growing urban agglomeration of Southern India. Environment, Development and Sustainability, doi: 10.1007/s10668-024-04494-9.

Kafy A A, Dey N N, Al Rakib A, et al. 2021a. Modeling the relationship between land use/land cover and land surface temperature in Dhaka, Bangladesh using CA-ANN algorithm. Environmental Challenges, 4: 100190, doi: 10.1016/j.envc.2021.100190.

Kafy A A, Rahman M S, Islam M, et al. 2021b. Prediction of seasonal urban thermal field variance index using machine learning algorithms in Cumilla, Bangladesh. Sustainable Cities and Society, 64: 102542, doi: 10.1016/j.scs.2020.102542.

Khan R, Aribam B, Alam W. 2023. Estimation of impacts of land use and land cover (LULC) changes on land surface temperature (LST) within greater Imphal urban area using geospatial technique. Acta Geophysica, 71(6): 2811–2823.

Komeh Z, Hamzeh S, Memarian H, et al. 2023. Monitoring the spatial autocorrelation of land surface temperature with land use in different climatic regions (case study: The metropolitans of Mashhad and Sari). Desert, 28(2): 329–351.

Krizhevsky A, Sutskever I, Hinton G E. 2012. Imagenet classification with deep convolutional neural networks. Advances in Neural Information Processing Systems, 25: 1097–1105.

Kumar L, Mutanga O. 2018. Google Earth Engine applications since inception: Usage, trends, and potential. Remote Sensing, 10(10): 1509, doi: 10.3390/rs10101509.

Kussul N, Lavreniuk M, Skakun S, et al. 2017. Deep learning classification of land cover and crop types using remote sensing data. IEEE Geoscience and Remote Sensing Letters, 14(5): 778–782.

Lausch A, Erasmi S, King D J, et al. 2017. Understanding forest health with remote sensing-part II–A review of approaches and data models. Remote Sensing, 9(2): 129, doi: 10.3390/rs9020129.

Lazzarini M, Marpu P R, Ghedira H. 2013. Temperature-land cover interactions: The inversion of urban heat island phenomenon in desert city areas. Remote Sensing of Environment, 130: 136–152.

Li M C, Ma L, Blaschke T, et al. 2016. A systematic comparison of different object-based classification techniques using high spatial resolution imagery in agricultural environments. International Journal of Applied Earth Observation and Geoinformation, 49: 87–98.

Li Y, Zhang H K, Shen Q. 2017. Spectral–spatial classification of hyperspectral imagery with 3D convolutional neural network. Remote Sensing, 9(1): 67, doi: 10.3390/rs9010067.

Li Z M, Chen B, Wu S B, et al. 2024. Deep learning for urban land use category classification: A review and experimental assessment. Remote Sensing of Environment, 311: 114290, doi: 10.1016/j.rse.2024.114290.

Liu J L, Liu S W, Tang X G, et al. 2022. The response of land surface temperature changes to the vegetation dynamics in the Yangtze River Basin. Remote Sensing, 14(20): 5093, doi: 10.3390/rs14205093.

Liu L, Zhang Y Z. 2011. Urban heat island analysis using the Landsat TM data and ASTER data: A case study in Hong Kong. Remote Sensing, 3(7): 1535–1552.

Ma L, Liu Y, Zhang X L, et al. 2019. Deep learning in remote sensing applications: A meta-analysis and review. ISPRS Journal of Photogrammetry and Remote Sensing, 152: 166–177.

Malik M S, Shukla J P, Mishra S. 2019. Relationship of LST, NDBI and NDVI using landsat-8 data in Kandaihimmat Watershed, Hoshangabad, India. Indian Journal of Geo-Marine Sciences, 48(1): 25–31.

Maxwell A E, Warner T A, Fang F. 2018. Implementation of machine-learning classification in remote sensing: An applied review. International Journal of Remote Sensing, 39(9): 2784–2817.

Mazzia V, Khaliq A, Chiaberge M. 2019. Improvement in land cover and crop classification based on temporal features learning from Sentinel-2 data using recurrent-convolutional neural network (R-CNN). Applied Sciences, 10(1): 238, doi: 10.3390/app10010238.

Memarian H, Balasundram S K, Khosla R. 2013. Comparison between pixel-and object-based image classification of a tropical

landscape using Système Pour l'Observation de la Terre-5 imagery. Journal of Applied Remote Sensing, 7(1): 073512, 10.1117/1.JRS.7.073512.

Munawar M, Prasetya T A E, McNeil R, et al. 2023. Spatio and temporal analysis of Indonesia land surface temperature variation during 2001–2020. Journal of the Indian Society of Remote Sensing, 51(7): 1393–1407.

Naidoo L, Van Deventer H, Ramoelo A, et al. 2019. Estimating above ground biomass as an indicator of carbon storage in vegetated wetlands of the grassland biome of South Africa. International Journal of Applied Earth Observation and Geoinformation, 78: 118–129.

Naushad R, Kaur T, Ghaderpour E. 2021. Deep transfer learning for land use and land cover classification: A comparative study. Sensors, 21(23): 8083, doi: 10.3390/s21238083.

Nega W, Balew A. 2022. The relationship between land use land cover and land surface temperature using remote sensing: Systematic reviews of studies globally over the past 5 years. Environmental Science and Pollution Research, 29(28): 42493–42508.

Patel S, Indraganti M, Jawarneh R N. 2023. A comprehensive systematic review: Impact of Land Use/Land Cover (LULC) on Land Surface Temperatures (LST) and outdoor thermal comfort. Building and Environment, 246: 111130, doi: 10.1016/j.buildenv.2023.111130.

Pérez G, Coma J, Sol S, et al. 2017. Green facade for energy savings in buildings: The influence of leaf area index and facade orientation on the shadow effect. Applied Energy, 187: 424–437.

Puissant A, Rougier S, Stumpf A. 2014. Object-oriented mapping of urban trees using Random Forest classifiers. International Journal of Applied Earth Observation and Geoinformation, 26: 235–245.

Qin Q, Dou J, Tu Z. 2020. Deep ResNet based remote sensing image super-resolution reconstruction in discrete wavelet domain. Pattern Recognition and Image Analysis, 30: 541–550.

Rahimpour M, Tajbakhsh M, Memarian H, et al. 2021. Impact assessment of climate change on hydro-climatic conditions of arid and semi-arid watersheds (case study: Zoshk-Abardeh watershed, Iran). Journal of Water and Climate Change, 12(2): 580–595.

Rasul A, Balzter H, Smith C. 2015. Spatial variation of the daytime surface urban cool island during the dry season in Erbil, Iraqi Kurdistan, from Landsat 8. Urban Climate, 14(2): 176–186.

Ravanelli R, Nascetti A, Cirigliano R V, et al. 2018. Monitoring the impact of land cover change on surface urban heat island through Google Earth Engine: Proposal of a global methodology, first applications and problems. Remote Sensing, 10(9): 1488, doi: 10.3390/rs10091488.

Rezaee M, Mahdianpari M, Zhang Y, et al. 2018. Deep convolutional neural network for complex wetland classification using optical remote sensing imagery. IEEE Journal of Selected Topics in Applied Earth Observations and Remote Sensing, 11(9): 3030–3039.

Rongali G, Keshari A K, Gosain A K, et al. 2018. A mono-window algorithm for land surface temperature estimation from Landsat 8 thermal infrared sensor data: A case study of the Beas River Basin, India. Pertanika Journal of Science & Technology, 26(2): 829–840.

Rosenzweig C, Karoly D, Vicarelli M, et al. 2008. Attributing physical and biological impacts to anthropogenic climate change. Nature, 453(7193): 353–357.

Schmidhuber J. 2015. Deep learning in neural networks: An overview. Neural Networks, 61: 85–117.

Shahfahad Kumari B, Tayyab M, Ahmed I A, et al. 2020. Longitudinal study of land surface temperature (LST) using mono-and split-window algorithms and its relationship with NDVI and NDBI over selected metro cities of India. Arabian Journal of Geosciences, 13: 1040, doi: 10.1007/s12517-020-06068-1.

Shin H C, Roth H R, Gao M C, et al. 2016. Deep convolutional neural networks for computer-aided detection: CNN architectures, dataset characteristics and transfer learning. IEEE Transactions on Medical Imaging, 35(5): 1285–1298.

Sidhu N, Pebesma E, Câmara G. 2018. Using Google Earth Engine to detect land cover change: Singapore as a use case. European Journal of Remote Sensing, 51(1): 486–500.

Tajbakhsh M, Memarian H, Shahrokhi Y. 2016. Analyzing and modeling urban sprawl and land use changes in a developing city using a CA-Markovian approach. Global Journal of Environmental Science and Management, 2(4): 397–410.

Tajbakhsh S, Memarian H, Moradi K, et al. 2018. Performance comparison of land change modeling techniques for land use projection of arid watersheds. Global Journal of Environmental Science and Management, 4(3): 263–280.

Taloor A K, Manhas D S, Kothyari G C. 2021. Retrieval of land surface temperature, normalized difference moisture index, normalized difference water index of the Ravi basin using Landsat data. Applied Computing and Geosciences, 9: 100051, doi: 10.1016/j.acags.2020.100051.

Tran D X, Pla F, Latorre-Carmona P, et al. 2017. Characterizing the relationship between land use land cover change and land

surface temperature. ISPRS Journal of Photogrammetry and Remote Sensing, 124: 119–132.

Tzotsos A, Argialas D. 2008. Support vector machine classification for object-based image analysis. In: Blaschke T, Lang S, Hay G. Object-Based Image Analysis: Spatial Concepts for Knowledge-Driven Remote Sensing Applications. Berlin: Springer, 663–677.

Vaglio Laurin G, Pirotti F, Callegari M, et al. 2016. Potential of ALOS2 and NDVI to estimate forest above-ground biomass, and comparison with lidar-derived estimates. Remote Sensing, 9(1): 18, doi: 10.3390/rs9010018.

Wang F, Qin Z H, Song C Y, et al. 2015. An improved mono-window algorithm for land surface temperature retrieval from Landsat 8 thermal infrared sensor data. Remote Sensing, 7(4): 4268–4289.

Wang J, Bretz M, Dewan M A A, et al. 2022. Machine learning in modelling land-use and land cover-change (LULCC): Current status, challenges and prospects. Science of the Total Environment, 822: 153559, doi: 10.1016/j.scitotenv.2022.153559.

Wang M M, Zhang Z J, Hu T, et al. 2019a. A practical single-channel algorithm for land surface temperature retrieval: application to landsat series data. Journal of Geophysical Research: Atmospheres, 124(1): 299–316.

Wang R, Cai M, Ren C, et al. 2019b. Detecting multi-temporal land cover change and land surface temperature in Pearl River Delta by adopting local climate zone. Urban Climate, 28: 100455, doi: 10.1016/j.uclim.2019.100455.

Wang Y, Fang Z C, Hong H Y. 2019c. Comparison of convolutional neural networks for landslide susceptibility mapping in Yanshan County, China. Science of the Total Environment, 666: 975–993.

Wang Y C, Hu B K, Myint S W, et al. 2018. Patterns of land change and their potential impacts on land surface temperature change in Yangon, Myanmar. Science of the Total Environment, 643: 738–750.

Xiong Y Z, Huang S P, Chen F, et al. 2012. The impacts of rapid urbanization on the thermal environment: A remote sensing study of Guangzhou, South China. Remote Sensing, 4(7): 2033–2056.

Yan G. 2003. Pixel Based and Object Oriented Image Analysis for Coal Fire Research. Enschede: ITC (Faculty of Geo-Information Science and Earth Observation).

Yengoh G T, Dent D, Olsson L, et al. 2015. Use of the Normalized Difference Vegetation Index (NDVI) to Assess Land Degradation at Multiple Scales: Current Status, Future Trends, and Practical Considerations. Berlin: Springer.

Zeraatkar Z, Shahidi A, Memarian Khalilabad H. 2021. Comparison of the accuracy of pixel-based and object-oriented methods in land use classification (case study: Samalghan Watershed). Journal of Natural Environment, 73(4): 687–700.

Zhan Q, Meng F, Xiao Y. 2015. Exploring the relationships of between land surface temperature, ground coverage ratio and building volume density in an urbanized environment. The International Archives of the Photogrammetry, Remote Sensing and Spatial Information Sciences, 40: 255–260.

Zhang L P, Zhang L F, Du B. 2016. Deep learning for remote sensing data: A technical tutorial on the state of the art. IEEE Geoscience and Remote Sensing Magazine, 4(2): 22–40.

Zhao H W, Chen Z X, Jiang H, et al. 2019. Evaluation of three deep learning models for early crop classification using sentinel-1A imagery time series–A case study in Zhanjiang, China. Remote Sensing, 11(22): 2673, doi: 10.3390/rs11222673.